Progress In Electromagnetics Research M, Vol. 113, 139–149, 2022

A Compact Dual-Band Circularly Polarized Antenna with Low Profile for BDS Applications

Gengliang Chen, Jingchun Zhai, Wen Wang, and Zhuopeng Wang*

Abstract—In this paper, a novel dual-frequency circularly polarized (CP) antenna applied to Beidou satellite (BDS) system is presented. CP radiation is achieved by etching slotted circular patches of complementary open-loop resonators, which are excited by a feeding network consisting of a double-layer power divider. The circular patch is miniaturized by a complementary split-ring resonator (CSRR) etched on the patch. The overall dimension of the antenna is only $0.32\lambda_0 \times 0.32\lambda_0 \times 0.0104\lambda_0$, where λ_0 is the corresponding free space wavelength at 1.268 GHz. The proposed antenna has 70 MHz (1.23–1.30 GHz) and 60 MHz (1.51–1.57 GHz) impedance bandwidth and 20 MHz (1.25–1.27 GHz) and 20 MHz (1.55–1.57 GHz) axial ratio bandwidth, respectively. The antenna profile is low, which is easy to install. Because of these performance indexes, the antenna has superior practicability in BDS system.

1. INTRODUCTION

In recent years, Beidou satellite (BDS) has been widely used in civil and military applications. The location service of a BDS system can be used in other navigation systems, so it has attracted extensive attention. With the improvement of application requirements, the requirements for BDS antenna are also developing toward miniaturization and multi-frequency. At the same time, the profile height also affects the size of the antenna, which is higher in the known literature. Therefore, in this context, this paper not only makes an in-depth study of miniaturization, multi-frequency compatibility, but also takes low profile as an important initial condition.

In the applications of BDS-2, the terminal needs to work in B3 and B1 bands, and has right hand circularly polarized (RHCP) radiation mode. In order to achieve dual-band [1, 2] RHCP, many studies have been done, including slot antenna [3, 4], cross dipole antenna [5, 6], and laminated microstrip patch antenna [7, 8]. For example, a single-fed dual-band circularly-polarized slot antenna is proposed in [3]. CP radiation can be realized by changing the width of the slot. A U-shaped dual-band circularly polarized antenna is proposed in [4]. In order to overcome the disadvantage of bidirectional radiation, metal reflectors are used to realize unidirectional radiation. In [5], a dual-band CP cross-asymmetric dipole antenna is proposed, and a cavity is used to obtain unidirectional radiation direction. In [7], a low-profile laminated dual-band CP microstrip antenna is proposed, which also has a very low frequency ratio and two narrow bandwidths about 1%.

The miniaturized dual-frequency circularly polarized antennas can be partitioned into three categories. Microstrip antenna is the most common category of miniaturized antenna. For example, high dielectric constant substrate is used in [9–11], placing a triangular slot diagonally on the patch radiator in [12], loading two short-circuit probes in parallel in [13], and a split-plate structure surrounded by a split-ring is used in [14]. Ring patch antenna is another method to reduce the measurement. In [15, 16], the orthogonal mode of a ring resonator is miniaturized by using a curved slot to excite it. Concentric ring in [17], rectangular ring in [18], and curved linear ring in [19] can be placed on different layers to

Received 30 July 2022, Accepted 1 September 2022, Scheduled 19 September 2022
* Corresponding author: Zhuopeng Wang (wzhuopeng1@sdust.edu.cn).
The authors are with the College of Electronic and Information Engineering, Shandong University of Science and Technology, China.

achieve miniaturization. In addition to the above two types, a variety of miniaturized dual-band CP cross dipole antennas have also been proposed. In [20], asymmetric barb arrows and printed inductors are embedded in the dipole to reduce the length of the base element and achieve dual frequencies. In [21, 22], a complementary split-ring resonator (CSRR) and four arms with different lengths are used to realize dual frequency operation and miniaturization. However, these cross dipole antennas usually require metal cavities, so their profiles are relatively high.

A miniaturized low profile dual frequency CP antenna is proposed in this paper. Four compact open fan-shaped patches are placed around the central patch, and the central patch etched on the arc-shaped gap is loaded with a CSRR, which is fed by a feed network consisting of a double-layer power divider, thus obtaining circularly polarized radiation. The compactness of the center patch and parasitic patch is realized by using short-circuit technology and meander technology. Section 2 introduces the design process of antenna in detail.

2. ANTENNA STRUCTURE

Figure 1 demonstrates the geometry configuration of the antenna. The antenna is composed of four portions: upper PCB, middle PCB, lower PCB, and connection structure (including feed pins and metal short circuit posts). The upper printed board is made of an FR4 substrate with a thickness of 1.6 mm, and the relative permittivity is 4.4. A slotted circular patch containing four complementary split ring resonators [23] is on the surface of the upper PCB. Four slotted fan-shaped patches are loaded around the center patch and connected to the ground through a metal short-circuit probe, so as to realize dual frequencies.

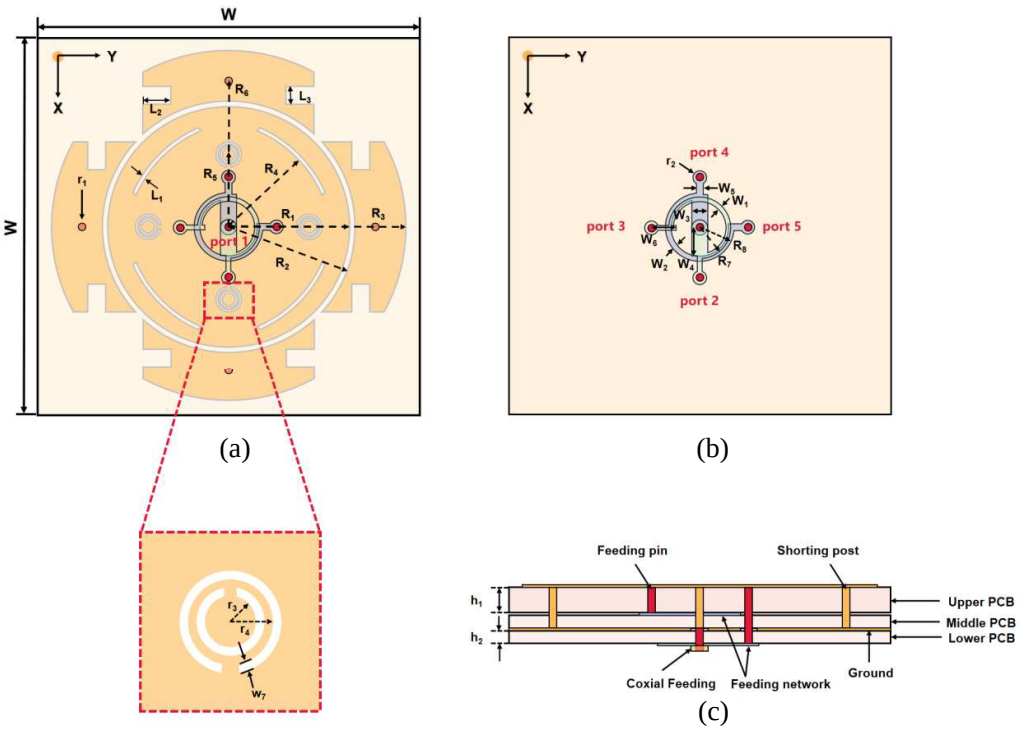

Figure 1. Antenna structure. (a) Vertical view. (b) Feeding network. (c) Lateral view.

The middle layer PCB and lower layer PCB [7, 8] adopt an FR4 substrate with thickness of 0.5 mm, and the relative permittivity is 4.4. The feeding network consists of two substrates and ground plane. A 50 Ω coaxial line is adopted in the input feeding structures. The outer conductor feeds the low PCB, while the inner conductor feeds to the middle PCB. Figure 2 exhibits the equivalent transmission line model of the feed network. The output difference of the power dividers of different layers is 180°. The

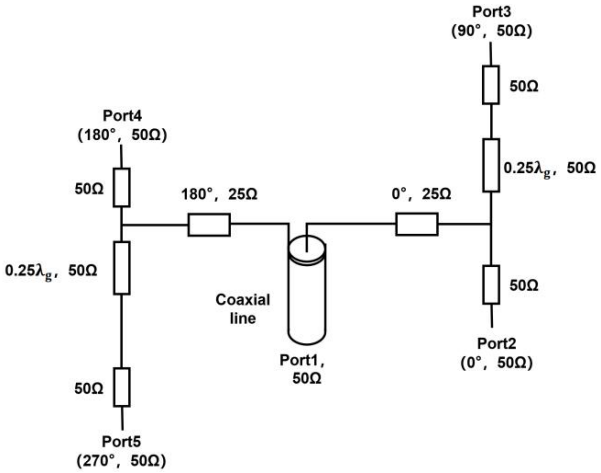

Figure 2. Equivalent transmission line model.

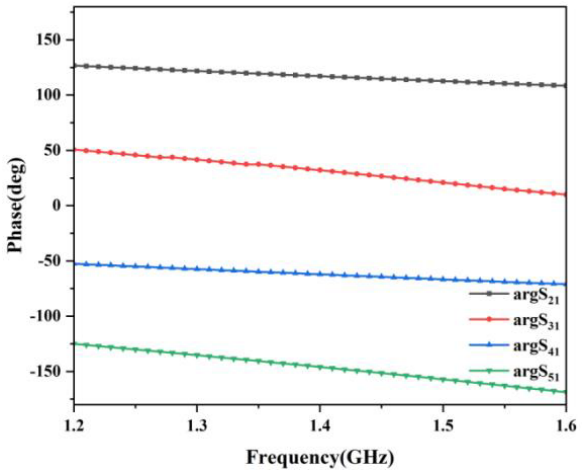

Figure 3. Phase difference of transmission coefficient.

output difference of the power divider in the same layer is 90° to achieve a 90° sequential difference among the four output ports of the feeding network.

As can be seen from Figure 3, the phase difference of transmission coefficient [24] between two adjacent ports varies within 90° ± 10° within the frequency band of 1.2 GHz–1.6 GHz. Therefore, the 90° phase shift characteristic of the feed network is good, which can ensure the antenna to obtain good right-handed circular polarization characteristic.

The phase difference caused by the three-quarters rings is different in different frequency bands. To adjust the phase difference of the power divider in different layers, the radius and width of the three-quarters rings are slightly different. The optimized antenna design parameters are shown in Table 1.

Table 1. The specific dimensions of the proposed antenna.

Parameter	R_1	R_2	R_3	R_4	R_5	R_6	R_7
Dimension (mm)	26.8	27.3	36.3	23.5	15	30.5	6
Parameter	R_8	L_1	L_2	L_3	W_1	W_2	W_3
Dimension (mm)	6.4	0.5	4	2	1	1.2	3
Parameter	W_4	W_5	W_6	W_7	r_1	r_2	r_3
Dimension (mm)	5.5	0.8	3	0.5	0.6	1.5	1
Parameter	r_4	W	h_1	h_2			
Dimension (mm)	2	80	1.6	0.5			

3. DESIGN PROCESS

Figure 4 exhibits the evolution procedure of the antenna. The original antenna is a common circular patch [25] with a resonant frequency of 1.55 GHz. Based on antenna A, parasitic fan-shaped patches [26] are loaded around the circular patch. Compared with antenna A, the resonant frequency of antenna B is shifted from 1.55 GHz to 1.48 GHz. In order to realize dual-frequency operation, a metal short-circuit probe is loaded on the parasitic fan-shaped patch to connect with the metal ground of the antenna, and the fan-shaped patch is changed to a fan-shaped patch with openings at both ends, so as to realize antenna C as shown in Figure 4. As can be seen from Figure 5, by loading the metal short-circuit probe [13], the antenna generates a new resonant frequency at 1.27 GHz in the low band, and the

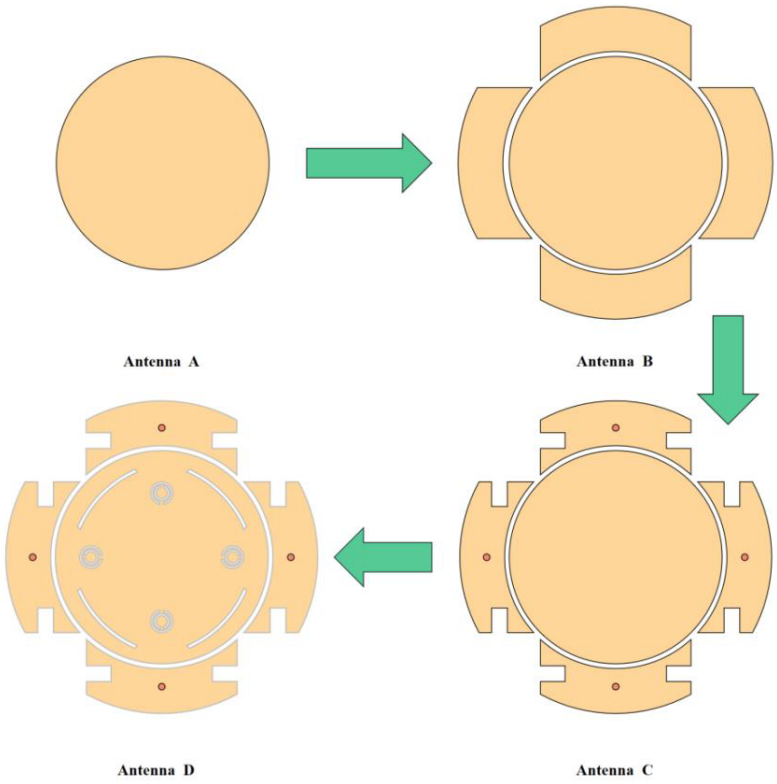

Figure 4. The design procedure of the proposed antenna.

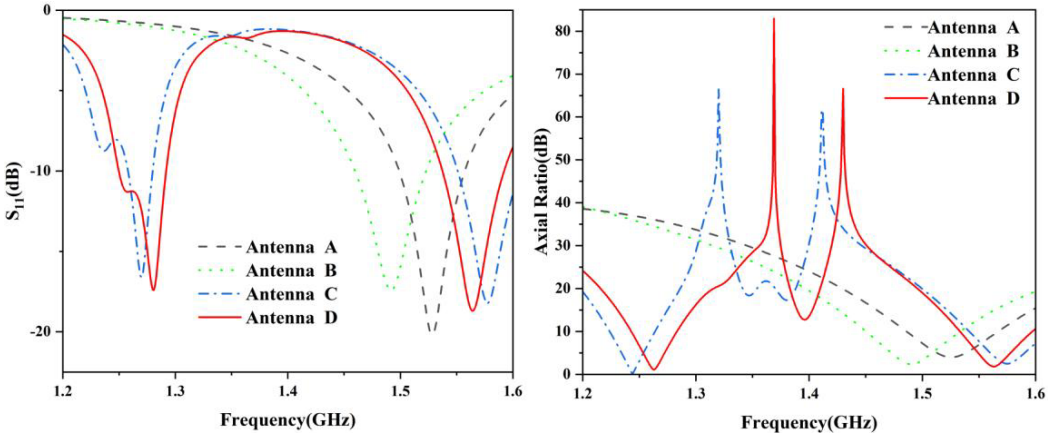

(a) S_{11} (b) AR

Figure 5. The simulation of the four antenna designs.

resonant frequency at 1.48 GHz shifts to 1.58 GHz in the high band. Finally, antenna C is loaded with an arc gap [3, 4] and CSRR to generate antenna D. As can be seen from Figure 5, the reflection coefficient in low frequency band is basically unchanged, and it drops from 1.58 GHz to 1.56 GHz in high frequency band. The antenna's axial ratio at 1.27 GHz and 1.56 GHz meets the requirements. Therefore, the complementary split-ring resonator not only realizes miniaturization, but also adjusts the axial ratio.

In the design, we use the following formula [25] to roughly calculate the size of the circular patch:

$$R_i \approx \frac{1.841 \cdot c}{2\pi\sqrt{\varepsilon_r} f_i} \tag{1}$$

$$R_1 \approx R_{1.56} \tag{2}$$

$$\Delta R \approx \sqrt{\frac{\pi R_{1.26}^2 - \pi R_{1.56}^2}{4\pi}} \tag{3}$$

$$R_3 \approx R_1 + \Delta R \tag{4}$$

Formula (1) is the relationship between the radius of the circular patch and the resonant frequency, where $i = 1.26, 1.56 \cdot c$ is the speed of light in vacuum, ε_r the effective dielectric constant, and f_i the resonant frequency of the patch in free space. R_1 is the radius of the center patch, R_3 the distance from the center of the circle to the parasitic fan-shaped patches, and ΔR the radius of the width of the parasitic fan-shaped patches.

We refer to Formula (1) to obtain the radius of the circular patch at 1.26 GHz and 1.56 GHz, respectively. Then, the area difference of the two patches is calculated, and $1/4\pi$ of the area difference is equivalent to the ΔR^2. According to the structure of the antenna, the circular patch at 1.26 GHz can be equivalent to the central patch and the loaded four parasites, so as to achieve dual frequencies. The calculated results are similar to the simulation ones.

The equivalent circuit of the CSRR loaded on the antenna surface is exhibited in Figure 6, which is represented as the parallel form of the LC resonant loop, and the resonant frequency of CSRR [23] is

$$f_0 = \frac{1}{2\pi\sqrt{L_r C_r}} \tag{5}$$

$$L_r = \frac{L_0}{4} \tag{6}$$

$$L_0 = 2\pi R L_p \tag{7}$$

where L_r is the inductance, C_r the capacitance, and L_p the inductance of unit length.

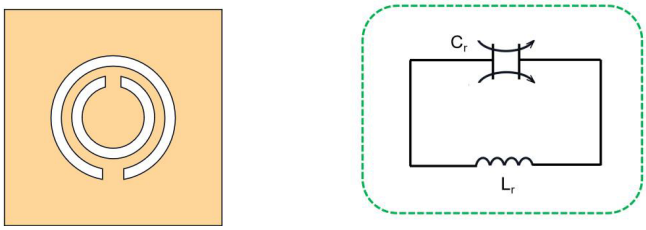

(a) CSRR structure (b) Equivalent circuit

Figure 6. CSRR structure and equivalent circuit diagram [23].

In order to verify the dual-frequency resonance characteristics of the antenna, the current distribution of antenna D at 1.268 GHz and 1.561 GHz is demonstrated in Figure 7. At 1.561 GHz, the antenna surface current is mainly concentrated on the central patch, which indicates that the resonance of the antenna at high frequency is mainly generated by the circular patch loaded with the complementary split-ring resonator. At 1.268 GHz, the antenna surface current is simultaneously distributed in the center patch and open fan-shaped patch, which proves that the resonance of the antenna at low frequency is jointly determined by the center patch and sector patch, and the surface current on the open fan-shaped patch is mainly generated by the coupling between the center patch and the antenna.

From the current distributions in Figures 8 and 9, it can be seen that the antenna works at 1.268 GHz and 1.568 GHz. In a complete cycle, the surface current distribution rotates counterclockwise from $+Z$ axis to $-Z$ axis. Thus, the antenna forms the radiation characteristic of right-handed circular polarization.

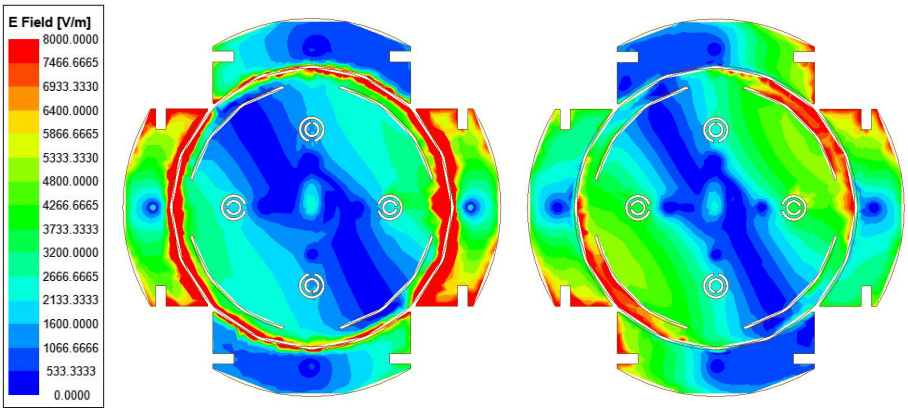

(a) 1.268 GHz (b) 1.561 GHz

Figure 7. Current distribution of antenna D at 1.268 GHz and 1.561 GHz.

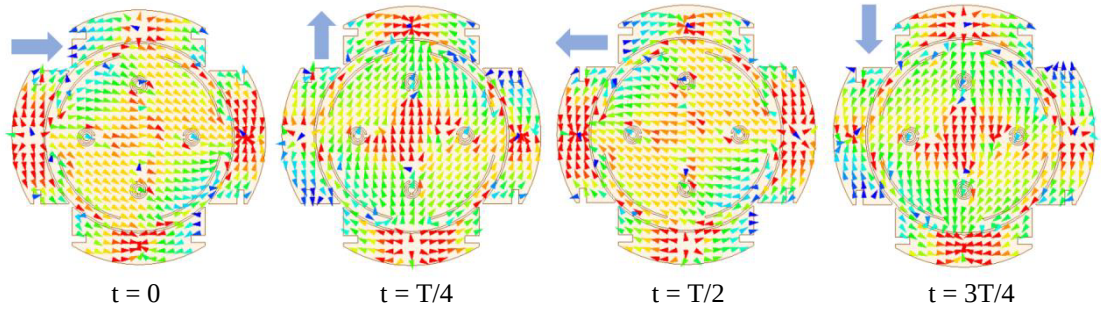

Figure 8. Current distribution of antenna at 1.268 GHz in one period.

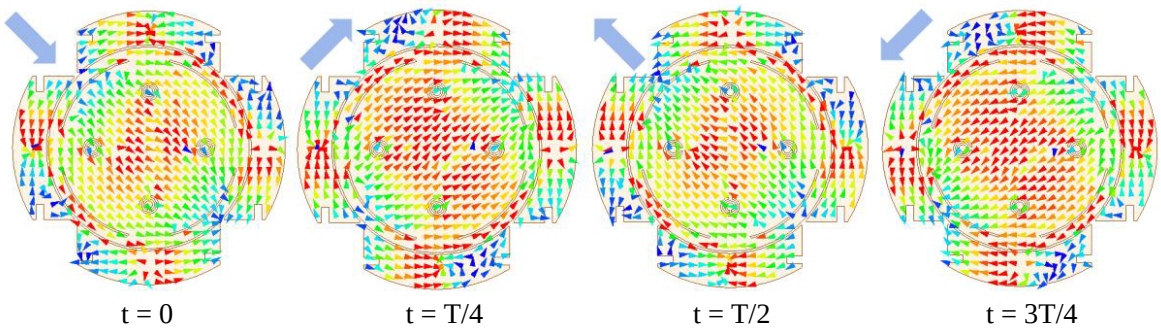

Figure 9. Current distribution of antenna at 1.561 GHz in one period.

4. PARAMETRIC STUDY

Figure 10 shows a simulation of S_{11} with different center patch sizes. As shown in Figure 10, when R_1 changes between 26.6 mm and 27.0 mm, the resonant frequency of low band decreases, while that of high band changes slightly, which can be basically regarded as stable at 1.56 GHz frequency point. According to the simulated S_{11} with different sizes, we choose $R_1 = 26.8$ mm as the size of the center patch.

Figure 11 shows a simulated S_{11} with different intervals between the central patch and parasitic patch. As shown in Figure 11, when R_2 changes between 27.1 mm and 27.5 mm, the resonant frequency of low band increases, while that of high band changes slightly, which can be basically regarded as

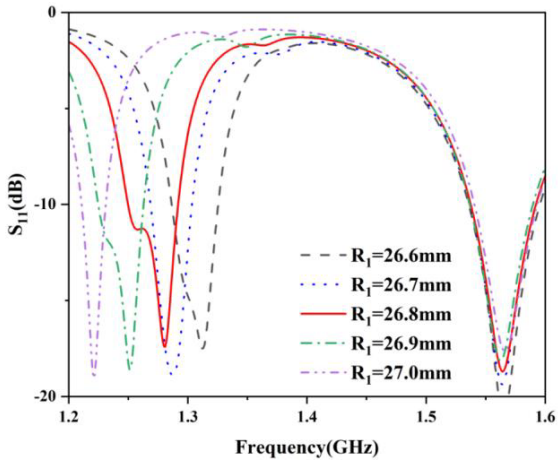

Figure 10. Simulated S_{11} for various values of R_1.

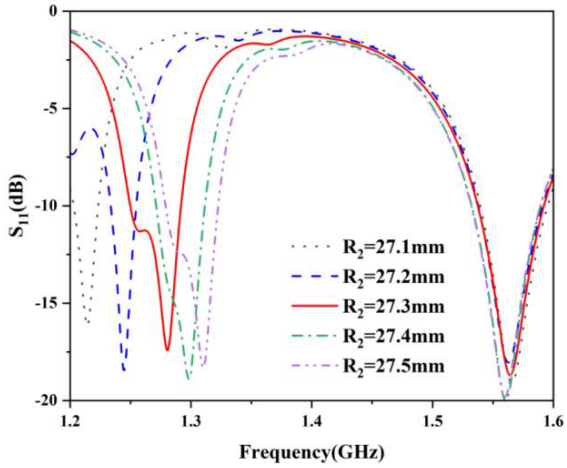

Figure 11. Simulated S_{11} for various values of R_2.

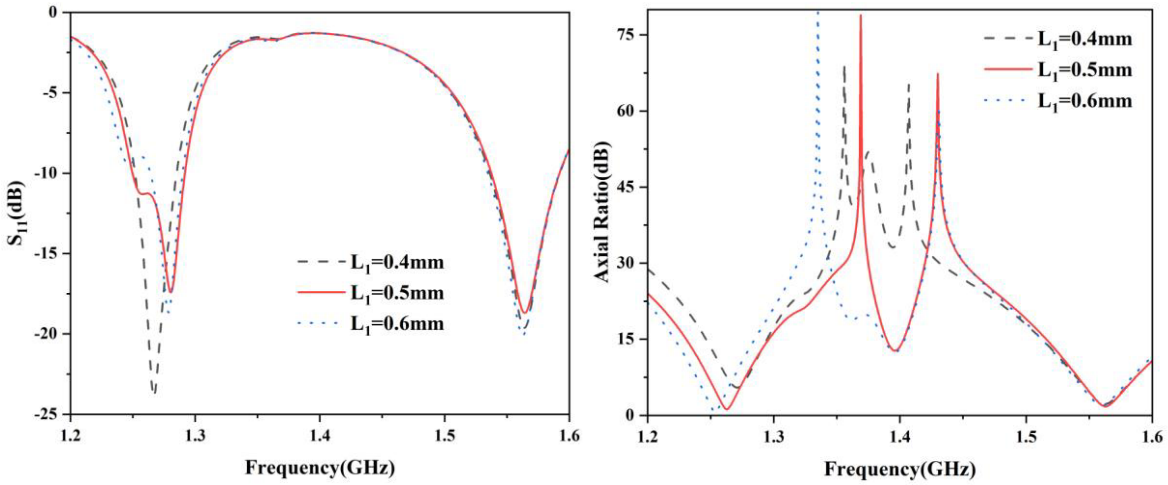

Figure 12. Simulated S_{11} and AR for various values of L_1.

stable at 1.56 GHz frequency point. This means that reducing the gap interval can increase the coupling capacitance formed between the parasitic patch and central patch, thus adjusting the resonance interval to the B1 and B3 bands.

Figure 12 shows simulated axial ratios with different gap intervals on the center patch. As shown in Figure 12, when L_1 changes between 0.4 mm and 0.6 mm, the frequency point at the high frequency is basically unchanged, while the position of the low frequency point will rise. It can be seen from the figure that when the gap interval is 0.5 mm, the axial ratio at low frequency of antenna can be better improved.

Figure 13 shows the simulation of S_{11} and axial ratio with the change of CSRR's outer radius. As shown in Figure 13, when r_4 varies between 2 and 3 mm, the low frequency point of the antenna gradually decreases, and when $r_4 = 2$ mm and 2.5 mm, the antenna's return loss in B3 band meets the requirements. As shown in Figure 13(b), when $r_4 = 2.5$ mm, the axial ratio at the low frequency point is the smallest, and the axial ratio will become larger when it is far from this value. Therefore, when adjusting the resonant frequency of B3 band by changing the outer radius of CSRR, the influence of the axial ratio of B3 band should also be taken into account.

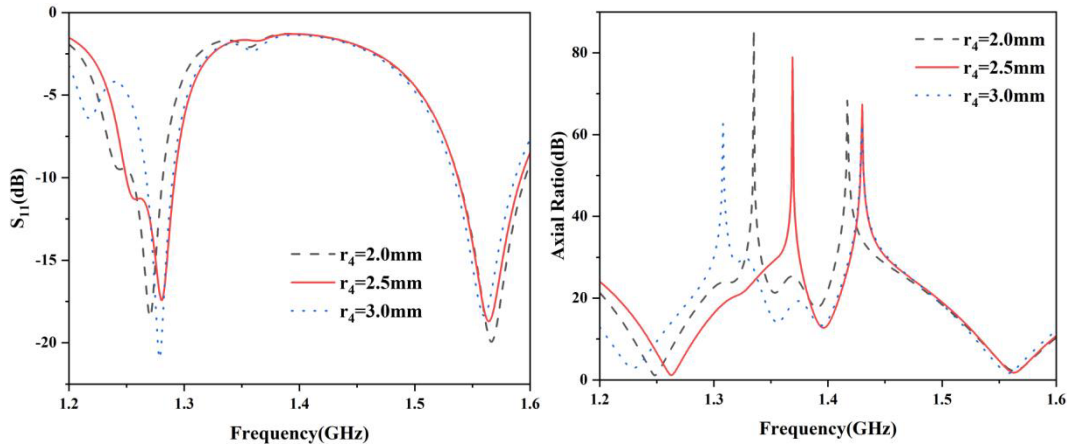

Figure 13. Simulated S_{11} and AR for various values of r_4.

5. SIMULATED AND MEASURED RESULTS

The proposed Beidou dual-band circularly polarized antenna is manufactured and measured, and the simulation results are verified. In Figure 14, the measured results of axial ratio and gain have good consistency with the simulation ones. The measurements meeting the design requirements show the impedance bandwidths of 70 MHz (1.23–1.30 GHz) and 60 MHz (1.51–1.57 GHz), and AR bandwidths of 20 MHz (1.25–1.27 GHz) and 20 MHz (1.55–1.57 GHz). Due to the errors in the manufacturing and measurement of the antenna, there are differences between the simulated and measured S_{11}, but the test results satisfy the design requirements of BDS antenna. We compare the antenna designed in this paper with other BDS antennas. We can see that not only the antenna designed in this paper realizes the miniaturization of the horizontal space direction, but also the profile height of the antenna is much lower than other antennas, which greatly reduces the size occupation of the antenna in the vertical space direction. A comparison of performance between the proposed antenna and other relevant papers is summarized in Table 2.

Figure 15 exhibits the simulated and measured radiation patterns of the right-handed circular polarization (main polarization) and left-handed circular polarization (cross polarization) in XOZ plane and YOZ plane when the antenna works at 1.268 GHz and 1.561 GHz in BDS-B3 band, respectively.

Table 2. Proposed antenna comparison with previous.

Antenna structure	Overall dimension	S_{11} bandwidth (%)	AR bandwidth (%)	HPBW (°)
[14]	$0.47\lambda_0 \times 0.42\lambda_0 \times 0.098\lambda_0$	12.7 11.4	1.9 2.1	≤ 80 ≤ 80
[19]	$0.45\lambda_0 \times 0.45\lambda_0 \times 0.077\lambda_0$	2.3 7.2	0.6 1.4	≤ 80 ≤ 80
[20]	$0.49\lambda_0 \times 0.49\lambda_0 \times 0.164\lambda_0$	6.3 22.0	1.9 7.3	≤ 80 ≤ 80
[22]	$0.37\lambda_0 \times 0.37\lambda_0 \times 0.122\lambda_0$	1.4 6.5	0.8 2.2	82 82
Proposed antenna	$0.32\lambda_0 \times 0.32\lambda_0 \times 0.0104\lambda_0$	5.6 3.9	1.6 1.2	101 90

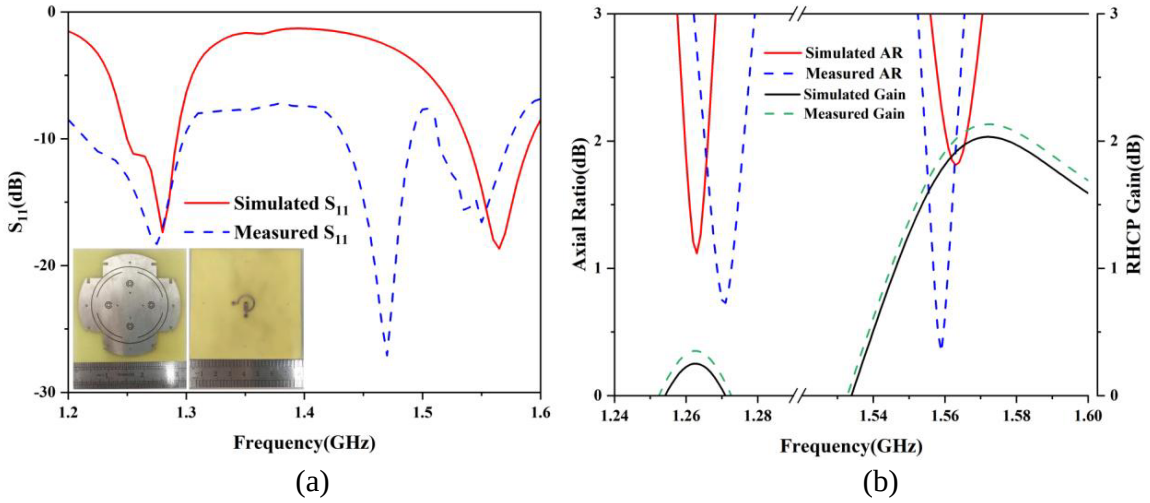

Figure 14. Simulated and Measured results, (a) S_{11}, (b) AR, RHCP Gain.

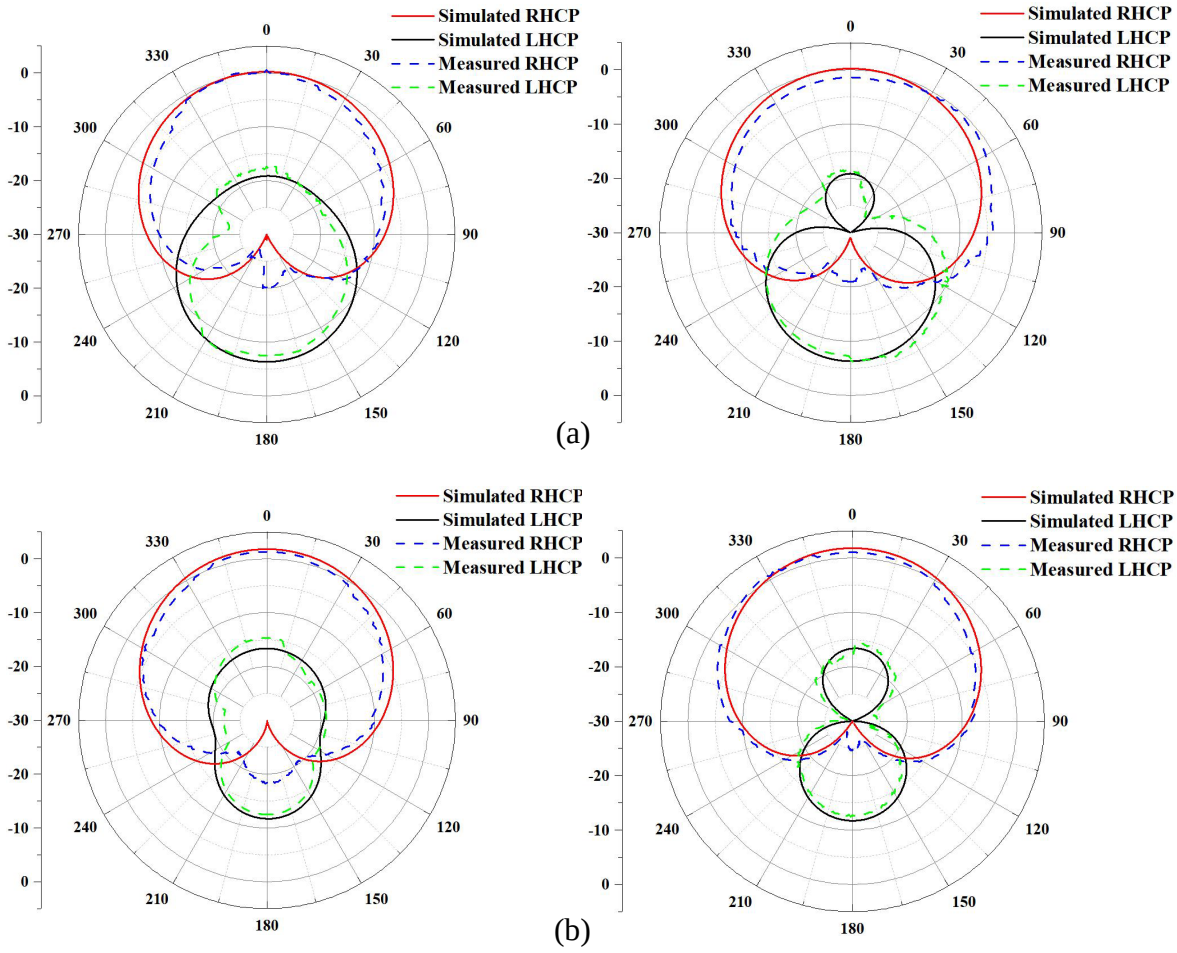

Figure 15. Simulated and Measured radiation patterns at (a) 1.268 GHz, (b) 1.561 GHz.

6. CONCLUSION

According to the application requirements of dual-band positioning of Beidou satellite navigation system, a miniaturized dual-frequency circularly polarized antenna working with BDS-B3 and BDS-B1 bands is proposed in this paper. The antenna has impedance bandwidths of 70 MHz (1.23–1.30 GHz) and 60 MHz (1.51–1.57 GHz), and AR bandwidths of 20 MHz (1.25–1.27 GHz) and 20 MHz (1.55–1.57 GHz), covering the B3 and B1 bands of BDS. Meanwhile, the overall dimension of the antenna is only $0.32\lambda_0 \times 0.32\lambda_0 \times 0.0104\lambda_0$, which significantly reduces the antenna size and lowers the cost. Because of these advantages, the proposed antenna is practical in Beidou satellite navigation.

REFERENCES

1. Chen, C.-H. and E. K. N. Yung, "A novel unidirectional dual-band circularly-polarized patch antenna," *IEEE Trans. Antennas Propag.*, Vol. 59, No. 8, 3052–3057, Aug. 2011.
2. Chang, T.-N., J.-M. Lin, and Y. G. Chen, "A circularly polarized ring-antenna fed by a serially coupled square slot-ring," *IEEE Trans. Antennas Propag.*, Vol. 60, No. 2, 1132–1135, Feb. 2012.
3. Cai, Y. M., S. F. Zheng, Y. Z. Yin, J. J. Xie, and K. Li, "Single-feed circularly polarized annular slot antenna for dual-broadband operation," *Progress In Electromagnetics Research C*, Vol. 39, 91–101, 2013.
4. Li, W.-M., B. Liu, and H.-W. Zhao, "The U-shaped structure in dual-band circularly polarized slot antenna design," *IEEE Antennas Wireless Propag. Lett.*, Vol. 13, 447–450, 2014.
5. Ta, S. X., I. Park, and R. W. Ziolkowski, "Dual-band wide-beam crossed asymmetric dipole antenna for GPS applications," *Eletronics Letters*, Vol. 48, No. 25, 1580–1581, 2012.
6. Lin, Y. F., Y. K. Wang, H. M. Chen, et al., "Circularly polarized crossed dipole antenna with phase delay lines for RFID handheld reader," *IEEE Trans. Antennas Propag.*, Vol. 60, No. 3, 1221–1227, 2012.
7. Su, C. M. and K. L. Wong, "A dual-band GPS microstrip antenna," *Microw. Opt. Technol. Lett.*, Vol. 33, No. 4, 238–240, 2002.
8. Ramírez, M. and J. Parrón, "Dual-band circularly polarized microstrip antenna," *Journal of Electromagnetic Waves and Applications*, Vol. 26, Nos. 5–6, 737–743, 2012, DOI: 10.1080/09205071.2012.710802.
9. Long, J. and D. F. Sievenpiper, "A compact broadband dual-polarized patch antenna for satellite communication/navigation applications," *IEEE Antennas Wireless Propag. Lett.*, Vol. 14, 273–276, 2015.
10. Chen, M. and C.-C. Chen, "A compact dual-band GPS antenna design," *IEEE Antennas Wireless Propag. Lett.*, Vol. 12, 245–248, 2013.
11. Gupta, S. and G. Mumcu, "Dual-band miniature coupled double loop GPS antenna loaded with lumped capacitors and inductive pins," *IEEE Trans. Antennas Propag.*, Vol. 61, No. 6, 2904–2910, 2013.
12. Nasimuddin, X. Qing, and Z. N. Chen, "A compact circularly polarized slotted patch antenna for GNSS applications," *IEEE Trans. Antennas Propag.*, Vol. 62, No. 12, 6506–6509, 2014.
13. Sun, C., H. Zheng, and Y. Liu, "Compact dual-band circularly polarised GNSS antenna," *Electronics Letters*, Vol. 51, No. 20, 1559–1560, 2015.
14. Chang, T. N. and J. M. Lin, "Corner-fed dual-band circularly polarised antenna," *IET Microwaves, Antennas & Propagation*, Vol. 8, No. 15, 1423–1431, 2014.
15. Zhang, K., C. Liu, X. Liu, H. Guo, and X. Yang, "Miniaturized circularly polarized implantable antenna for ISM-band biomedical devices," *International Journal of Antennas and Propagation*, Vol. 2017, Article ID 9750257, 9 pages, 2017.
16. Li, Y., S. Sun, and F. Yang, "A miniaturized Yagi-Uda-oriented double-ring antenna with circular polarization and directional pattern," *IEEE Antennas Wireless Propag. Lett.*, Vol. 12, 945–948, 2013.

17. Ramirez, M., J. Parron, J. M. Gonzalez-Arbesu, and J. Gemio, "Concentric annular-ring microstrip antenna with circular polarization," *IEEE Antennas Wireless Propag. Lett.*, Vol. 10, 517–519, 2011.
18. Li, Y., B. Tian, J. Xue, and G. Ge, "Compact dual-band circularly polarized antenna design for navigation terminals," *IEEE Antennas Wireless Propag. Lett.*, Vol. 15, 802–805, 2016.
19. Chen, K., J. Yuan, and X. Luo, "Compact dual-band dual circularly polarised annular-ring patch antenna for BeiDou Navigation Satellite System application," *IET Microwaves, Antennas & Propagation*, Vol. 11, No. 8, 1079–1085, 2017.
20. Ta, S. X., I. Park, and R. W. Ziolkowski, "Dual-band wide-beam crossed asymmetric dipole antenna for GPS applications," *Electronics Letters*, Vol. 48, No. 25, 1580–1581, 2012.
21. Saurav, K., D. Sarkar, and K. V. Srivastava, "Dual-band circularly polarized cavity-backed crossed-dipole antennas," *IEEE Antennas Wireless Propag. Lett.*, Vol. 14, 52–55, 2015.
22. Ta, S. X. and I. Park, "Dual-band operation of a circularly polarized four-arm curl antenna with asymmetric arm length," *International Journal of Antennas and Propagation*, Vol. 2016, Article ID 3531089, 10 pages, 2016.
23. Yue, T., et al., "A compact dual-band antenna enabled by a complementary split-ring resonator-loaded metasurface," *IEEE Trans. Antennas Propag.*, Vol. 65, No. 12, 6878–6888, 2017.
24. Li, C., F. Zhang, F. Zhang, and K. Yang, "A dual-band circularly polarized antenna with wide HPBWs for CNSS applications," *IEICE Electronics Express*, 1–10, 2018.
25. Garg, R., *Microstrip Antenna Design HandBook*, Artechhouse, USA, 2001.
26. Tanabe, M., "A circular HIS reflector with a symmetric fan-shape patch array applied to a spiral antenna," *2021 IEEE-APS Topical Conference on Antennas and Propagation in Wireless Communications (APWC)*, 1–3, 2021.